SUPPLEMENATRY INFORMATION

for

Photophysical Properties of Thermally Activated Delayed Fluorescent Materials upon Distortion of Central Axis of Donor Moiety

Hyung Suk Kim [a], Hansol Park [a], So-Ra Park [a], Sang Hoon Lee [a], Yunho Ahn [a], Yong Sup Lee [b], and Min Chul Suh [a,]*

[a]Department of Information Display, Kyung Hee University, Seoul 02447, Republic of Korea
[b]Department of Life and Nanopharmaceutical Sciences, College of Pharmacy, Kyung Hee University, Seoul 02447, Republic of Korea

Corresponding Author
*E-mail: mcsuh@khu.ac.kr

Appendix. Theoretical background for TADF behavior

Early research[1-3] provided the strategy that minimizes ΔE_{ST} to realize TADF character. This corresponds to separating spatial wave function between HOMO and LUMO, under the premise where the main electron configuration (i.e., S_1 and T_1 states) corresponds to transition from HOMO to LUMO. In this regard, the control of exchange energy (J) has been the key rule to destabilize S_1 state and stabilize T_1 state to the same extent, leading to the value of $\Delta E_{ST} = 2J$.[4-6] However, small ΔE_{ST} by reducing J results in a negative effect for k_r^s. The transition dipole moment, from S_1 to the ground state (S_0), relies on the oscillator strength (f). In conclusion, low k_r^s is in line with the low PLQY of TADF molecule. Recently, RISC mechanism, supported by the three electronic states (S_1, T_1, and S_0), could be more interpreted by locally triplet excited state (^{3}LE).[7-9] Within the framework of Fermi's golden rule,[10-12] k_{RISC} can be expressed as follows

$$k_{\mathrm{RISC}} = \frac{2\pi}{\hbar}\left|\widehat{\mathcal{H}}_{\mathrm{SOC}}^{\mathrm{S_1T_1}}\right|^2 \rho_{\mathrm{FC}}$$

Eq. (S1)

where $\widehat{\mathcal{H}}_{\mathrm{SOC}}^{\mathrm{S_1T_1}} = \langle \mathrm{T_1}|\widehat{\mathcal{H}}_{\mathrm{SOC}}|\mathrm{S_1}\rangle$ is the SOCME between T_1 and S_1 adiabatic electronic states. ρ_{FC} denotes the Franck-Condon weighted density of states (FCWD)[13] given by

$$\sum_j \sum_k e^{-\frac{E_j}{k_B T}} \langle \nu_k^{final} | \nu_j^{inital} \rangle^2 \delta(E_j^{initial} - E_k^{final})$$

Eq. (S2)

Where j and k denote the vibrational state. k_B is defined as Boltzmann constant and T is the temperature. An introduction of the canonical partition function ($e^{-\frac{E_j}{k_B T}}$) for vibration motion in the initial electronic state can support Arrhenius-type equation in the high-temperature region. $\langle \nu_k^{final} | \nu_j^{inital} \rangle$ corresponds to overlap between the vibrational wave functions. Delta function (δ) ensures the energy conservation for the non-radiative transition. E_j and E_k denominate the vibrational energy level in the initial and final electronic state, respectively.[14-

[16] ρ_{FC} obeys a standard Arrhenius relationship in high *T* regime[14], which implies that ρ_{FC} is decreasing the function of ΔE_{ST}. Thus, k_{RISC} could take its semi-classical *Marcus* theory expression.[12-14,17-20] (*vide infra*)

$$\sqrt{\frac{1}{4\pi k_B T \lambda_s}} \sum_{n=0}^{\infty} e^{-S} \frac{S^n}{n!} e^{-\frac{(\Delta E_{ST} + \lambda_M + n\hbar\omega_{eff})^2}{4k_B T \lambda_s}}$$

Eq. (S3)

Herein, *Marcus* reorganization energy (λ_s) is associated with intermolecular and intramolecular classical low-frequency modes. $\hbar\omega_{eff}$ is the effective energy of a mode involved in transition (non-classical high frequency intramolecular vibrational mode). *S* is the effective *Huang-Rhys* factor related to the mentioned modes. An advanced calculation, based on Condon framework (**Eq. S1**) with **Eq. S3** performed by Jean-Luc Brédas *et al.*[12], provided that strong SOCME value and a small ΔE_{ST} could make the value of k_{RISC} achieve ~ 10^8 s^{-1}. This can be also possible albeit SOCME is relatively much smaller than that of phosphorescent material. The first-order perturbation theory could strongly support direct SOC between states (^{3}CT-^{1}CT and ^{3}LE-^{1}CT) but not include fast equilibrium between triplet states (^{3}LE-^{3}CT). Under the framework of this theory, the mixing between T_1 and T_2 states can be established (*vide infra*)[21]

$$T_2(\,^3\Psi_{LE}) = \,^3\Psi_{LE} + \frac{\langle\,^3\Psi_{LE}|\widehat{\mathcal{H}}_{Vib}|\,^3\Psi_{CT}\rangle}{^3E_{LE} - \,^3E_{CT}}$$

Eq. (S4)

The spin-vibronic coupling between ^{3}LE and ^{3}CT leads to rapid formation of an equilibrium between two states (i.e., non-adiabatic). Thus, ^{3}LE state has been dealt with as an essential factor to modulate the photophysical property of TADF material. The actual system (^{3}CT coupled to ^{1}CT) can be dissected by the second-order perturbation theory (**Eq. S5**):[8,16,21-22]

$$k_{\mathrm{RISC}} = \frac{2\pi}{\hbar}\left| \langle {}^{1}\Psi_{\mathrm{CT}} | \hat{\mathcal{H}}_{\mathrm{SOC}} | {}^{3}\Psi_{\mathrm{CT}} \rangle + \frac{\langle {}^{1}\Psi_{\mathrm{CT}} | \hat{\mathcal{H}}_{\mathrm{SOC}} | {}^{3}\Psi_{\mathrm{LE}} \rangle \langle {}^{3}\Psi_{\mathrm{LE}} | \hat{\mathcal{H}}_{Vib} | {}^{3}\Psi_{\mathrm{CT}} \rangle}{{}^{3}\mathrm{E}_{\mathrm{LE}} - {}^{3}\mathrm{E}_{\mathrm{CT}}} \right|^{2} \delta({}^{3}\mathrm{E}_{\mathrm{CT}} - {}^{1}\mathrm{E}_{\mathrm{CT}})$$

Eq. (S5)

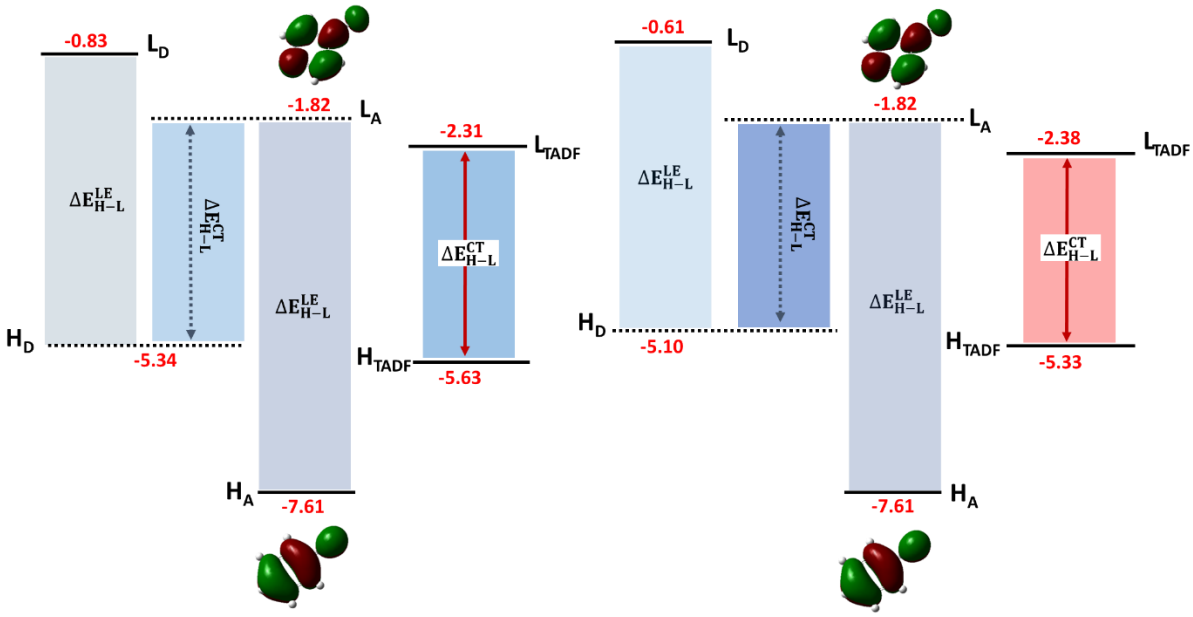

Figure S1. Schematic illustration of the HOMO-LUMO energy gap for the donor, acceptor moieties and donor-acceptor-donor TADF molecule. H_D (H_A) and L_D (L_A) corresponds to the HOMO and LUMO of the donor (acceptor) unit, respectively. ΔE^{CT}_{H-L} (dotted line) is denoted as the energy gap between H_D and L_A. Calculated bandgaps ($\Delta E^{CT}_{H-L} = L_{TADF} - H_{TADF}$, solid line) based on TD-DFT at BL3YP hybrid functional and 6-311+G(d). HOMO and LUMO orbital distribution for **BN** moiety was depicted.

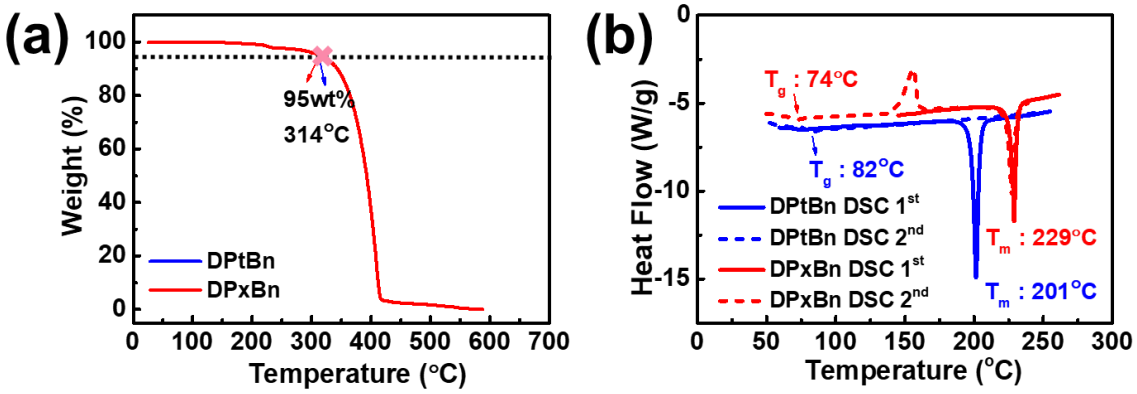

Figure S2. (a) TGA (b) DSC traces of DPtBn, and DPxBn.

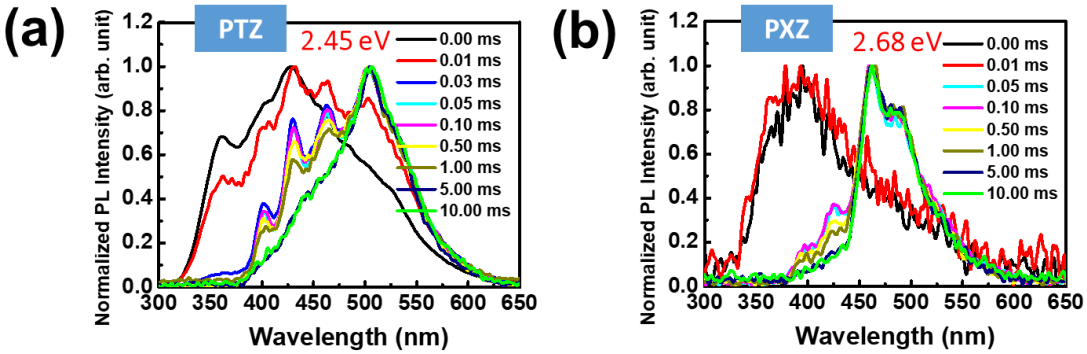

Figure S3. Phosphorescence spectra (concentration, 1.0 x 10^{-4} M in toluene) for PTZ and PXZ donor units within timescale (from 0 to 10 ms) at 77 K and tabulated $^{3}LE_s$ levels.

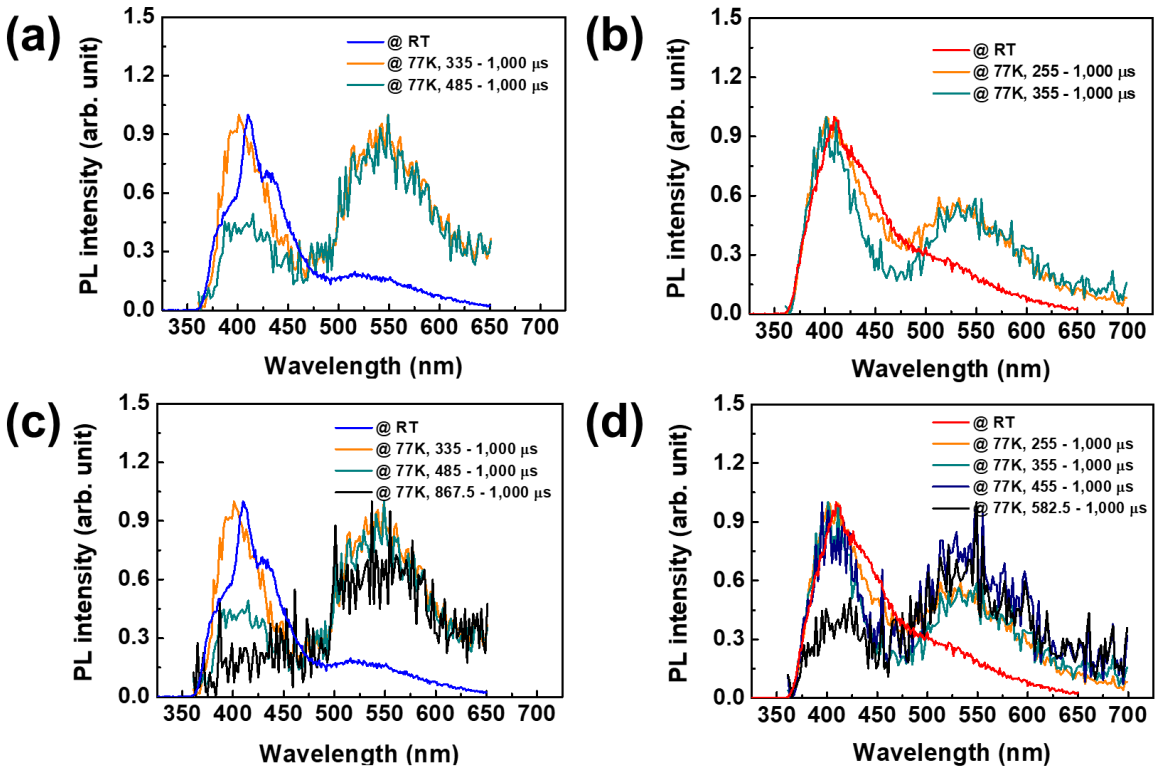

Figure S4. Phosphorescence spectra for PTZ (a) and PXZ (b) donor units condensed in *m*-CBP solid film (doping concentration, 5 wt %; film thickness, 30 nm). $^{3}LE_{f}$ was estimated from Tr-PL decay of spectrum collected at 2 nm interval using TCSPC method at 77K (method, Cryostat equipment). And, λ_{ex} was 340 nm. The black solid line from (c) and (d) clearly supports the long phosphorescence spectrum of each donor moiety in the solid state window.

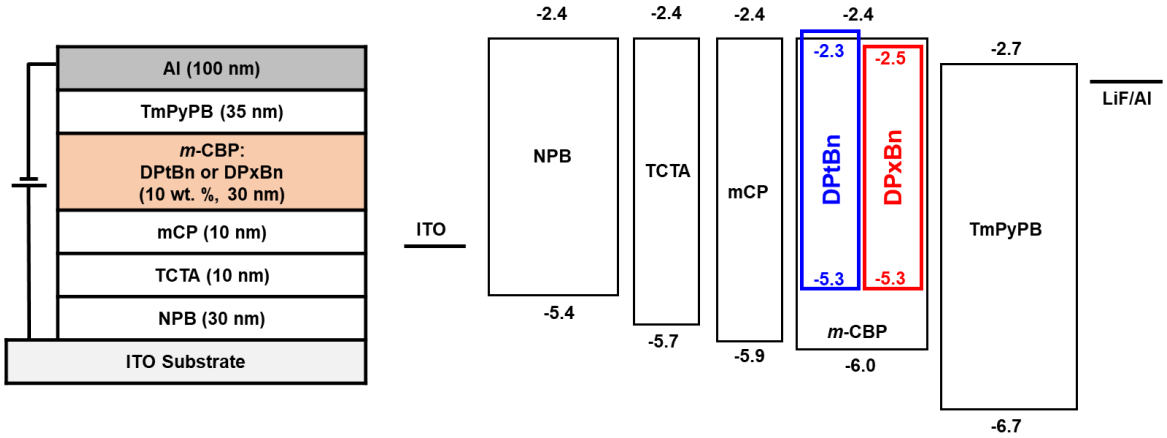

Figure S5. Schematic of the device architecture (left) and energy diagram of the OLEDs utilized in this work (right).

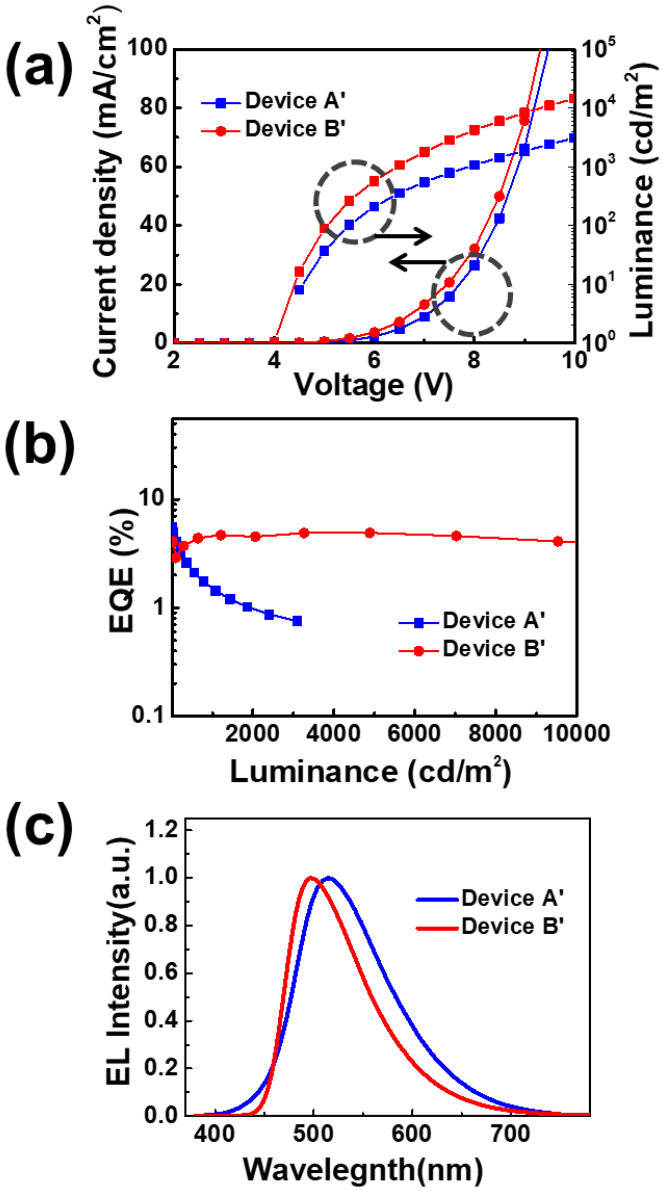

Figure S6. (a) *J-V-L* (b) EQE-luminance curves, and (c) EL profiles for device A' and B', respectively

Table S1. The DFT/TD-DFT Results Based on B3LYP Hybrid Functional

target TADF	S_1[a,b] [eV]	T_1[a,b] [eV]	f[a,b]	HOMO[a] [eV]	LUMO[a] [eV]	α[a] [°]
DPtBn	2.69	2.64	0.0004	-5.55	-2.20	106.2
DPxBn	2.31	2.27	0.0001	-5.22	-2.25	96.9

[a]The ground state geometries of DPtBn and DPxBn were optimized at the B3LYP/6-311G(d) level in the gas phase. [b]The configurations and energies in the excited states and oscillator strength (*f*) were calculated using TD-DFT at B3LYP/6-311+G(d).

Table S2. The DFT/TD-DFT Results Based on PBE_0 Hybrid Functional

target TADF	S_1[a,b] [eV]	T_1[a,b] [eV]	f[a,b]	HOMO[a] [eV]	LUMO[a] [eV]	α[a] [°]
DPtBn	2.83	2.75	0.0005	-5.74	-2.09	109.0
DPxBn	2.50	2.43	0.0001	-5.42	-2.09	97.4

[a]The ground state geometries of DPtBn and DPxBn were optimized at the PBE0/6-311G(d) level in the gas phase. [b]The configurations and energies in the excited states and *f* were calculated using TD-DFT at PBE0/6-311+G(d).

Table S3. The DFT/TD-DFT Results Based on LC-*w*PBE Long-Range Corrected Exchange-Correlation Functional

target TADF	S_1[a,b] [eV]	T_1[a,b] [eV]	f[a,b]	HOMO[a] [eV]	LUMO[a] [eV]	α[a] [°]
DPtBn	2.46	2.42	0.0004	-5.55	-2.20	106.2
DPxBn	2.47	2.42	0.0001	-5.22	-2.25	96.9

[a]The ground state geometries of DPtBn and DPxBn were optimized at the B3LYP/6-311G(d) level in the gas phase. [b]The configurations and energies in the excited states and *f* were calculated using TD-DFT at LC-*w*PBE/6-311+G(d) where the parameter *w* was 0.11 and 0.15 for DPtBn and DPxBn, respectively

Table S4. The DFT/TD-DFT Results Based on LC-*w*PBE Long-Range Corrected Exchange-Correlation Functional

target TADF	S_1[a,b] [eV]	T_1[a,b] [eV]	f[a,b]	HOMO[a] [eV]	LUMO[a] [eV]	α[a] [°]
DPtBn	2.37	2.33	0.0006	-5.53	-2.24	109.9
DPxBn	2.42	2.34	0.0005	-5.26	-2.18	109.4

[a]The ground state geometries of DPtBn and DPxBn were optimized at the LC-*w*PBE/6-311G(d) level in the gas phase (*w* = 0.05). [b]The configurations and energies in the excited states and *f* were calculated using TD-DFT at LC-*w*PBE/6-311+G(d) where the parameter *w* was 0.11 and 0.14 for DPtBn and DPxBn, respectively.

Table S5. The DFT/TD-DFT Results Based on LC-*w*PBE Long-Range Corrected Exchange-Correlation Functional with Solvation Model Based on Density (SMD)

target TADF	S_1[a,b] [eV]	T_1[a,b] [eV]	f[a,b]	HOMO[a] [eV]	LUMO[a] [eV]	α[a] [°]
DPtBn	2.43	2.39	0.0006	-5.54	-2.06	107.2
DPxBn	2.51	2.45	0.0002	-5.13	-2.07	100.0

[a]The ground state geometries of DPtBn and DPxBn were optimized at the SMD/LC-*w*PBE/6-311G(d) level dissolved in the toluene (w = 0.05). [b]The configurations and energies in the excited states and f were calculated using TD-DFT at SMD/LC-*w*PBE/6-311+G(d) where the parameter w was 0.11 and 0.15 for DPtBn and DPxBn, respectively.

Table S6. Summary of OLEDs Device with Target TADF (DPtBn, DPxBn) Emitter

item	V_{on}[a]/V_{op}[b](V)	CE//PE//EQE (cd/A//lm/W//%)		CIE (x,y)[b]
		maximum	at 1000 cd/m^2	
device A′	4.1/7.9	16.0/11.2/5.6	4.3/1.7/1.5	(0.30,0.49)
device B′	3.9/6.4	15.6/9.1/4.9	14.9/7.3/4.6	(0.24,0.45)

[a] Measured at 1 cd/m^2. [b] Measured at 1,000 cd/m^2.

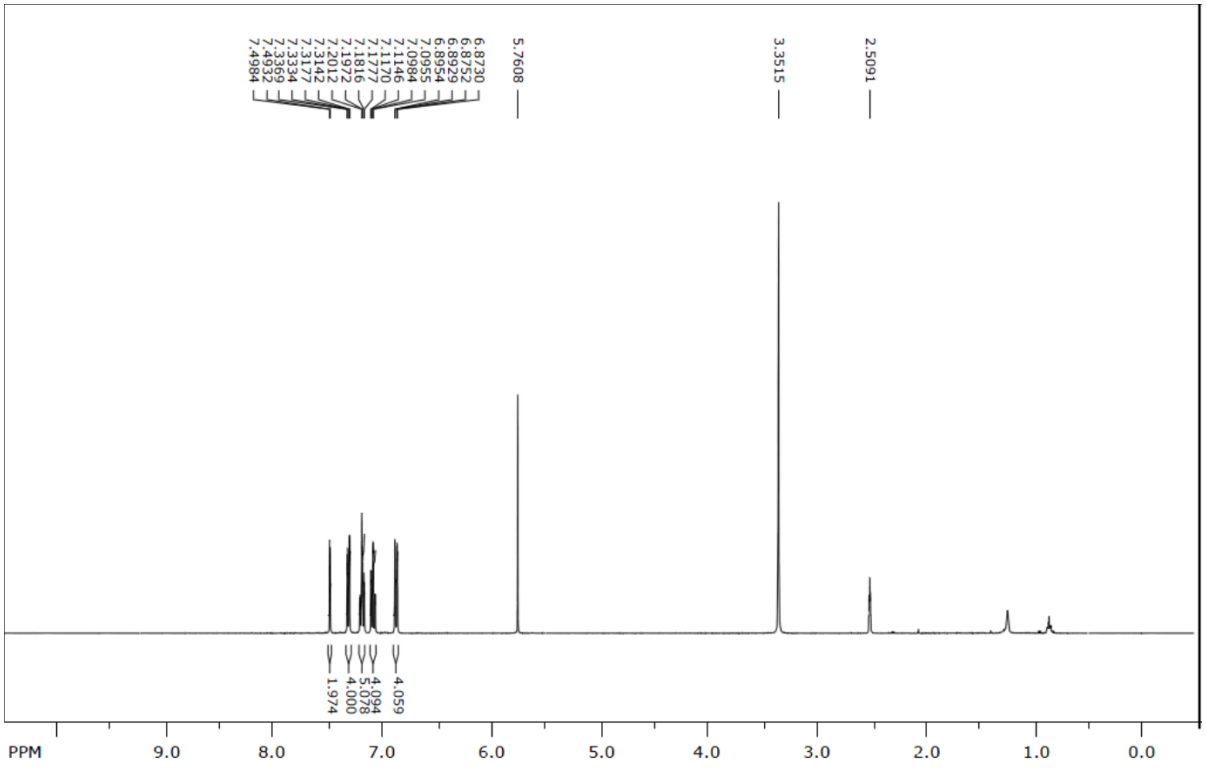

Figure S7. ^{1}H NMR spectrum of DPtBn

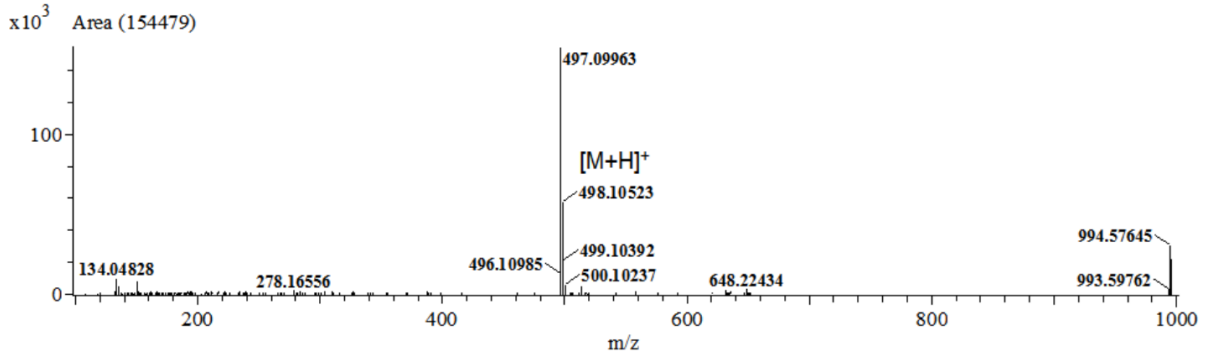

Figure S8. HR-MS spectrum of DPtBn

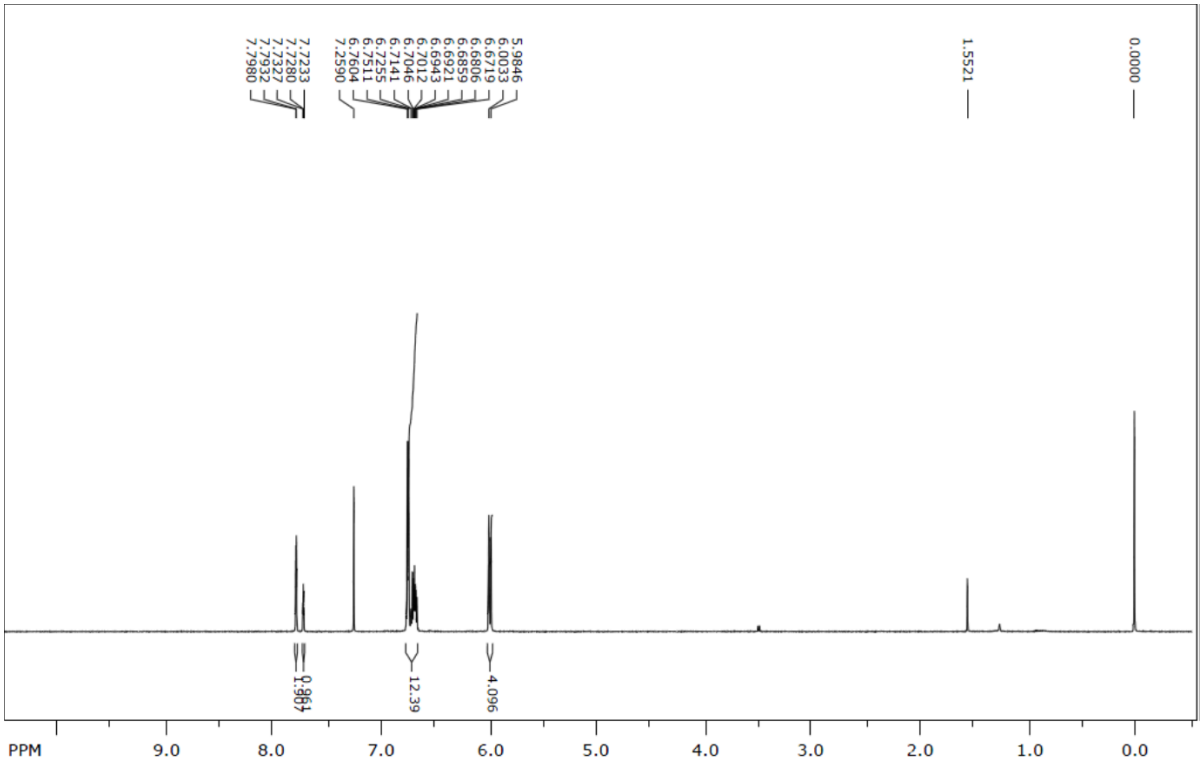

Figure S9. ^{1}H NMR spectrum of DPxBn.

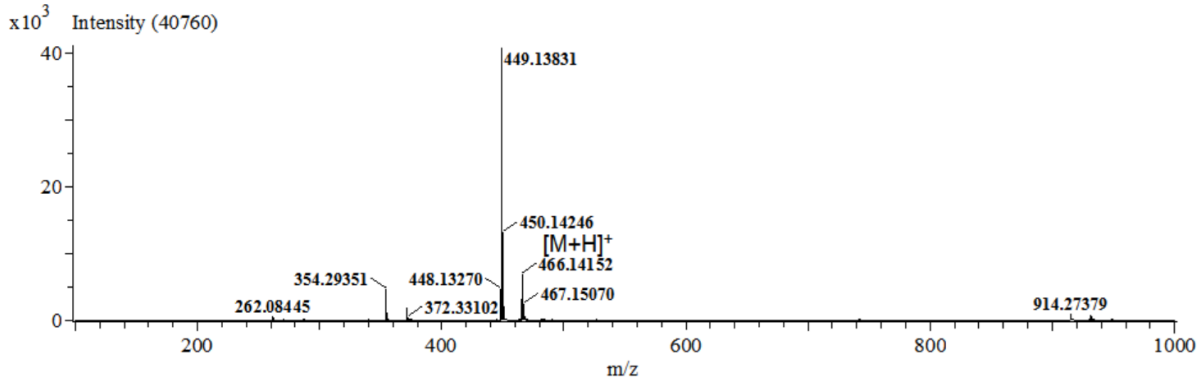

Figure S10. HR-MS spectrum of DPxBn.

REFERENCE

[1] Hirata, S.; Sakai, Y.; Masui, K.; Tanaka, H.; Lee, S. Y.; Nomura, H.; Nakamura, N.; Yasumatsu, M.; Nakanotani, H.; Zhang, Q.; et al. Highly Efficient Blue Electroluminescence based on Thermally Activated Delayed Fluorescence *Nat. Mater.* **2015**, 14, 330336.

[2] Sato, K.; Shizu, K.; Yoshimura, K.; Kawada, H.; Miyazaki, Adachi. C. Organic Luminescent Molecule with Energetically Equivalent Singlet and Triplet Excited States for Organic Light-Emitting Diodes. *Phys. Rev. Lett.* **2013**, 110, 247401.

[3] Wong, M. Y.; Zysman-Colman, E. Purely Organic Thermally Activated Delayed Fluorescence Materials for Organic Light-Emitting Diodes. *Adv. Mater*. **2017**, 29, 1605444.

[4] Tao, Y.; Yuan, K.; Chen, T.; Xu, P.; Li, H. Chen, R.; Zheng, C.; Zhang, L.; Huang. W. Thermally Activated Delayed Fluorescence Materials Towards the Breakthrough of Organoelectronics. *Adv. Mater*. **2014**, 26, 7931-7958.

[5] Yang, Z.; Mao, Z.; Xie, Z.; Zhang, Y.; Liu, S.; Zhao, J.; Xu, J.; Chi, Z.; Aldred, M. P. Recent Advances in Organic Thermally Activated Delayed Fluorescence Materials. *Chem. Soc. Rev*. **2017**, 47, 915-1016.

[6] Köhler, A.; Bässler, H. Triplet States in Organic Semiconductors. *Mater. Sci. Eng., R* **2009**, 66, 71-109.

[7] Dias, F. B.; Santos, J.; Graves, D. R.; Data, P.; Nobuyase, R. S.; Fox, M. A.; Batsanov, A. S.; Palmeira, T.; Berberan-Santos, M. N.; Bryce, M. R.; et al. The Role of Local Triplet Excited States and D-A Relative Orientation in Thermally Activated Delayed Fluorescence: Photophysics and Devices. *Adv. Sci*. **2016**, 3, 1600080.

[8] Etherignton, M. K.; Gibson, J.; Higginbotham, H. F.; Penfold, T. J.; Monkman, A. P. Revealing the Spin–Vibronic Coupling Mechanism of Thermally Activated Delayed Fluorescence. *Nat. Commun*. **2016**, 7, 13680.

[9] Nobuyasu, R. S.; Ren, Z.; Griffiths, G. C.; Batsanov, A. S.; Data, P.; Yan, S.; Monkman, A. P.; Bryce, M. R.; Dias, F. B. Rational Design of TADF Polymers Using a Donor–Acceptor Monomer with Enhanced TADF Efficiency Induced by the Energy Alignment of Charge Transfer and Local Triplet Excited States. *Adv. Opt. Mater.* **2016**, 4, 597-607.

[10] Lawetz, V.; Siebrand, W.; Orlandi, G. Theory of Intersystem Crossing in Aromatic Hydrocarbons *J. Chem. Phys.* **1972**, 56, 4058-4072.

[11] Robinson, G. W.; Frosch, R. P. Electronic Excitation Transfer and Relaxation. *J. Chem. Phys.* **1963**, 38, 1187-1203.

[12] Samanta, P. K.; Kim, D.; Coropceanu, V.; Brédas, J. –L. Up-Conversion Intersystem Crossing Rates in Organic Emitters for Thermally Activated Delayed Fluorescence: Impact of the Nature of Singlet vs Triplet Excited States. *J. Am. Chem. Soc.* **2017**, 139, 4042-4051.

[13] Chen, X. K.; Zhang, S. F.; Fan, J. X.; Ren, A. M. Nature of Highly Efficient Thermally Activated Delayed Fluorescence in Organic Light-Emitting Diode Emitters: Nonadiabatic Effect between Excited States. *J. Phys. Chem. C* **2015**, 119, 9728-9733.

[14] Marian, C. M. Spin–Orbit Coupling and Intersystem Crossing in Molecules *Mol. Sci*. **2012**, 2, 187−203.

[15] Rice, O. K. Perturbations in Molecules and the Theory of Predissociation and Diffuse Spectra. II *Phys. Rev*. **1930**, 35, 1551−1558.

[16] Dias, F. B.; Penfold, T. J.; Monkman, A. P. Photophysics of Thermally Activated Delayed Fluorescence Molecules. *Methods Appl. Fluoresc.* **2017**, 5, 012001.

[17] Brédas, J. –L.; Belijonne, D.; Coropceanu, V.; Cornil, J. Charge-Transfer and Energy-Transfer Processes in π-Conjugated Oligomers and Polymers: A Molecular Picture. *Chem. Rev.* **2004**, 104, 4971-5003.

[18] Schmidt, K.; Brovelli, S.; Coropceanu, V.; Belijonne, D.; Cornil, J.; Bazzini, C.; Caronna, T.; Tubino, R.; Meinardi, F.; Shuai, Z.; Brédas, J. –L. Intersystem Crossing Processes in Nonplanar Aromatic Heterocyclic Molecules. *J. Phys. Chem. A* **2007**, 111, 10490-10499.

[19] Gibson, J.; Monkman, A. P.; Penfold, T. J. The Importance of Vibronic Coupling for Efficient Reverse Intersystem Crossing in Thermally Activated Delayed Fluorescence Molecules. *ChemPhysChem* **2016**, 17, 2956-2961.

[20] Marcus, R. A. Nonadiabatic Processes Involving Quantum-Like and Classical-Like Coordinates with Applications to Nonadiabatic Electron Transfers. *J. Chem. Phys.* **1984**, 81, 4494-4500.

[21] Gibson, J.; Penfold, T. J. Nonadiabatic Coupling Reduces the Activation Energy in Thermally Activated Delayed Fluorescence. *Phys. Chem. Chem. Phys.* **2017**, 19, 8428-8434.

[22] Henry, B. R.; Siebrand, W. Spin–Orbit Coupling in Aromatic Hydrocarbons. Analysis of Nonradiative Transitions between Singlet and Triplet States in Benzene and Naphthalene. *J. Chem. Phys*. **1971**, 54, 1072.